ACS OMEGA

Open Access

http://pubs.acs.org/journal/acsodf

Article

Phosphatase and Pseudo-Phosphatase Functions of Phosphatase of Regenerating Liver 3 (PRL-3) Are Insensitive to Divalent Metals In Vitro

Jeffery T. Jolly, Ty C. Cheatham, and Jessica S. Blackburn*

Cite This: *ACS Omega* 2023, 8, 30578−30589

Read Online

ACCESS | Metrics & More | Article Recommendations | Supporting Information

ABSTRACT: Phosphatase of regenerating liver 3 (PRL-3) is associated with cancer metastasis and has been shown to interact with the cyclin and CBS domain divalent metal cation transport mediator (CNNM) family of proteins to regulate the intracellular concentration of magnesium and other divalent metals. Despite PRL-3's importance in cancer, factors that regulate PRL-3's phosphatase activity and its interactions with CNNM proteins remain unknown. Here, we show that divalent metal ions, including magnesium, calcium, and manganese, have no impact on PRL-3's structure, stability, phosphatase activity, or CNNM binding capacity, indicating that PRL-3 does not act as a metal sensor, despite its interaction with CNNM metal transporters. In vitro approaches found that PRL-3 is a broad but not indiscriminate phosphatase, with activity toward di- and tri-nucleotides, phosphoinositols, and NADPH but not other common metabolites. Although calcium, magnesium, manganese, and zinc-binding sites were predicted near the PRL-3 active site, these divalent metals did not specifically alter PRL-3's phosphatase activity toward a generic substrate, its transition from an inactive phospho-cysteine intermediate state, or its direct binding with the CBS domain of CNNM. PRL-3's insensitivity to metal cations negates the possibility of its role as an intracellular metal content sensor for regulating CNNM activity. Further investigation is warranted to define the regulatory mechanisms governing PRL-3's phosphatase activity and CNNM interactions, as these findings could hold potential therapeutic implications in cancer treatment.

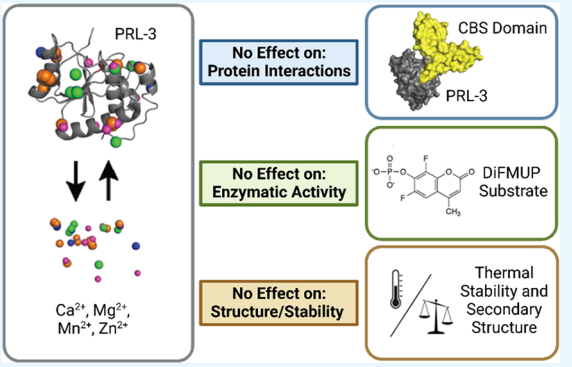

1. INTRODUCTION

The phosphatase of regenerating liver (PRL) protein family consists of three highly conserved dual-specificity phosphatases that are localized to the plasma membrane by their C-terminal prenylation motif.[1] Among the family members, PRL-3 has been extensively studied due to its association with cancer metastasis. PRL-3 was first identified as a protein of interest in 2001 when its expression was found to be significantly elevated in metastatic colorectal cancer compared to non-metastatic samples. This discovery presented the possibility of PRL-3 as a prognostic marker and indicator of metastatic potential.[2] Subsequent studies have established the involvement of PRL-3 in metastasis and a poor patient prognosis in various cancer types, including breast, gastric, liver, ovarian, prostate, leukemia, and others, confirming the clinical importance of this phosphatase.[3−7] In addition to its potential as a prognostic marker, PRL-3 has been shown to actively contribute to cancer-promoting cellular phenotypes, including proliferation, motility, cell survival, cytokinesis, angiogenesis, metabolism, and many others, illustrating the extent of the interplay between PRL-3 and the numerous mechanisms that contribute to an oncogenic phenotype.[8−12]

In addition to their phosphatase activity, the PRL family tightly binds cystathionine β-synthase (CBS) domains of the cyclin and CBS domain divalent metal cation transport mediator (CNNM) family of proteins.[13−16] The CNNM family consists of four membrane-localized proteins that mediate the transport of divalent metals directly or through interactions with ion channels, such as TRPM7.[17−21] The interaction between the PRLs and CNNM proteins promotes intracellular accumulation of magnesium, which drives signaling pathways associated with metastasis.[22−24] Disruption of this interaction diminishes the oncogenic effects of the PRLs in vitro. This pseudo-phosphatase function is also important for PRL-3-mediated metastatic phenotypes in vivo, as demonstrated through DB-7 and B16 cancer models in syngeneic mice.[23,25] Consequently, the regulatory mechanisms governing

Received: June 9, 2023
Accepted: July 26, 2023
Published: August 9, 2023

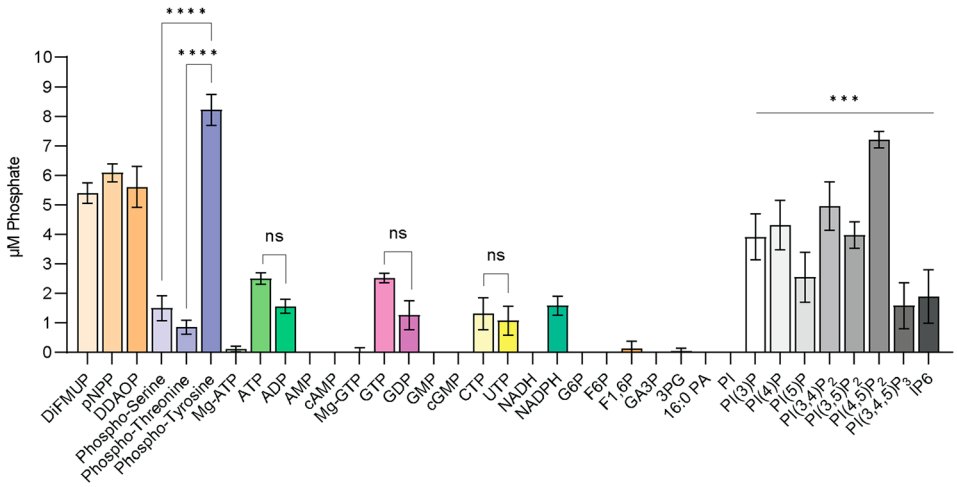

Figure 1. PRL-3 can dephosphorylate numerous non-protein substrates. A malachite green assay was used to determine if PRL-3 could dephosphorylate the indicated synthetic substrates, amino acids, nucleotides, metabolites, and phospholipids. The amount of inorganic phosphate released after 1.5 h incubation was calculated from a standard curve. Error bars represent the standard deviation. Significance was calculated using an ordinary one-way analysis of variance (ANOVA) analysis. ****$p < 0.0001$, comparing PRL-3 activity against phospho-tyrosine to phospho-serine and phospho-threonine, ***$p < 0.001$, comparing PRL-3 activity against PI(4,5)P_2 to the other phosphatidylinositol substrates, ns = no significant difference.

the interaction between PRL and CNNM proteins are a topic of significant interest.

A known regulator of the PRL:CNNM interaction is the enzymatic activity of the PRLs. Following the initial dephosphorylation of a substrate, the PRLs assume a phospho-cysteine intermediate state due to the slow release of the phosphate from the catalytic cysteine residue.[26] While in this intermediate form, the PRLs cannot bind the CBS domains of CNNMs.[15] Notably, the proportion of PRLs existing in the active state versus the enzymatic intermediate state appears to vary across different cell types, but the reason for this is unknown. Most PRL-1 and 2 exists in the phospho-cysteine intermediate state within mouse heart, liver, and skeletal muscle tissue, whereas the ratio is more evenly distributed in colon tissue.[15,23] Similarly, within human embryonic kidney and cervical cancer (HeLa) cell lines, PRLs primarily exist in the inactive phospho-cysteine intermediate form under normal media conditions. However, upon removing magnesium from the media, there is a significant increase in the abundance of non-phosphorylated PRL proteins. Upon re-introduction of magnesium to the media, the PRLs rapidly reverted into the phospho-cysteine intermediate state, where they would no longer be able to bind CNNMs.[15,23] Adding to this complexity, PRL-3 mRNA contains a magnesium-sensitive sequence that promotes translation in response to low magnesium levels.[27,28] This finding provides a potential mechanism for the role of PRLs in magnesium homeostasis within the cell. However, it currently is unclear if translational regulation can entirely account for the rapid changes in PRL phosphorylation seen in response to altered magnesium levels in vitro. Other post-translational modifications or factors that impact PRL's enzymatic activity may be responsible for the rapid activation and inhibition of PRLs within the cell.

We postulated that fluctuating intracellular metal concentrations could directly alter the PRL-3:CNNM interaction and allow PRL-3 to serve as a metal sensor. Metal ions exhibit diverse roles as obligate cofactors or enhancers of enzymatic activity and potent inhibitors of catalytic functions. In addition, they can exert profound effects on protein structure and serve as crucial regulators of protein interaction.[29] Regarding PRL-3, metal ions could enhance the typically slow enzymatic rate of the protein or, conversely, act as inhibitors of PRL-3 function. This dual effect has been commonly observed in other phosphatases, such as alkaline phosphatase and protein tyrosine phosphatase 1B (PTP1B).[30,31] Metal ions could regulate the PRL-3:CNNM interaction through two potential mechanisms: first, metal ions might bind to PRL-3 and trigger conformational changes that affect its stability and structure, thereby inhibiting its interaction with the CBS domain. Second, metal ions might directly modulate the enzymatic activity of PRL-3 to regulate the availability of the enzyme for binding to CNNMs. Either of these functions could serve as a direct mechanism, by which PRL-3 could serve as a sensor of intracellular metal concentrations and respond accordingly to maintain homeostasis. Considering the emerging roles of interactions between CNNMs and TRPM7, an ion channel protein that can regulate numerous cations outside of magnesium,[21,32−34] we decided to explore the regulatory effects of calcium, magnesium, manganese, and zinc ions on PRL-3 activity.

In this study, we identified potential metal binding sites on PRL-3 in silico and tested the impact of metal ions on various properties of the enzyme, including secondary structure, thermal stability, phosphatase activity, and CNNM binding capacity. Although Zn^{2+} had a non-specific destabilizing effect on the protein, Ca^{2+}, Mg^{2+}, and Mn^{2+} had no discernable impact on the tested properties of PRL-3. This observation suggests that alternative cellular mechanisms, such as PRL-3's post-translational modifications or fluctuations in substrate availability, may predominantly regulate the PRL-3:CNNM interaction rather than PRL-3 itself directly functioning as a sensor of intracellular metal concentrations.

2. RESULTS

2.1. PRL-3 Can Dephosphorylate Numerous Cellular Moieties. In addition to its recognized protein substrates, PRL-3 has been reported to have phosphatase activity against

https://doi.org/10.1021/acsomega.3c04095
ACS Omega 2023, 8, 30578−30589

numerous cellular targets, including nucleotides and phosphoinositides.[16,35] To comprehensively investigate the specificity of PRL-3 against non-protein substrates, we used a malachite green assay to screen a wide range of phosphorylated synthetic compounds, amino acids, nucleotides, metabolites, and inositol lipids as potential substrates. We observed that many of these compounds could serve as substrates for PRL-3 (Figure 1).

As expected, small synthetic compounds such as DiFMUP, pNPP, and DDAOP were readily dephosphorylated. PRL-3 exhibited phosphatase activity against phospho-serine, phospho-threonine, and phospho-tyrosine, with a significant preference for the latter. Regarding the nucleotides, our findings align with previous reports and demonstrate that PRL-3 displays no specificity outside of diphosphate bonds, while the presence of magnesium could inhibit the dephosphorylation of Mg-ATP and Mg-GTP.[16] Interestingly, PRL-3 had no significant enzymatic activity against the screened metabolites except NADPH. However, PRL-3 had enzymatic activity against all the phospholipids and the IP6 headgroup, albeit with varying activity levels. Consistent with previous observations, we confirmed that PRL-3 prefers PI(4,5)P_2 over any other phospholipid.[35] We extended our investigation to the other PRL family members (PRL-1 and PRL-2) and found similar enzymatic profiles for these phosphatases (Figure S1). Given the abundance of potential cellular substrates, we sought to determine whether fluctuating metal concentrations could impact PRL-3's function.

2.2. PRL-3 Has Multiple Predicted Metal Binding Sites. Enzymatic and crystallography studies indicate that PRL-3 and its interaction with CNNMs do not strictly depend on metal ions,[16] but metals might exert modulatory effects on these properties. Given the role of PRLs in regulating magnesium and other metals in the cells via interaction with CNNM/TRPM7,[36] we sought to determine if metal ions could interact with PRL-3 and impact its function. In silico modeling using Protein Data Bank (PDB) structures5TSR[16] and 1V3A[37] predicted 10−15 potential binding sites for calcium, magnesium, manganese, and zinc ions on PRL-3, and each metal ion had at least one predicted site near the PRL-3/CNNM3 interface. In addition, multiple metal binding sites were identified near the PRL-3 active site and the WPD loop, a critical region for PRL-3 phosphatase activity (Figure 2). A summary of the top five predicted binding sites for each metal for either PDB entry is shown in Table S1. These computational models suggest that metals have the potential to alter PRL-3 function. Given these predictions, we next wanted to determine if metal ions could affect the biochemical properties of PRL-3.

2.3. Calcium, Magnesium, and Manganese Ions Do Not Alter the Secondary Structure of PRL-3, but Zinc Ions Have a Denaturing Effect. We used circular dichroism (CD) spectroscopy to screen for PRL-3 secondary structure changes in the presence of the metal ions. The generated CD spectra from samples containing 25 μM metal salts are shown in Figure 3A. In both the control buffer and buffer containing 125 μM EDTA, the secondary structure of PRL-3 was estimated to consist of 50% alpha-helix, 27% beta-sheet, 21% turns, and 2% other or unstructured and was essentially unchanged with the addition of $CaCl_2$, $MgCl_2$, and $MnCl_2$ with the secondary structure estimations only varying by ∼4−6% for each component. We found that $ZnCl_2$ had a denaturing effect on the protein in a dose-dependent manner, as 25 μM $ZnCl_2$ had a greater destabilizing effect than 5 μM $ZnCl_2$, as

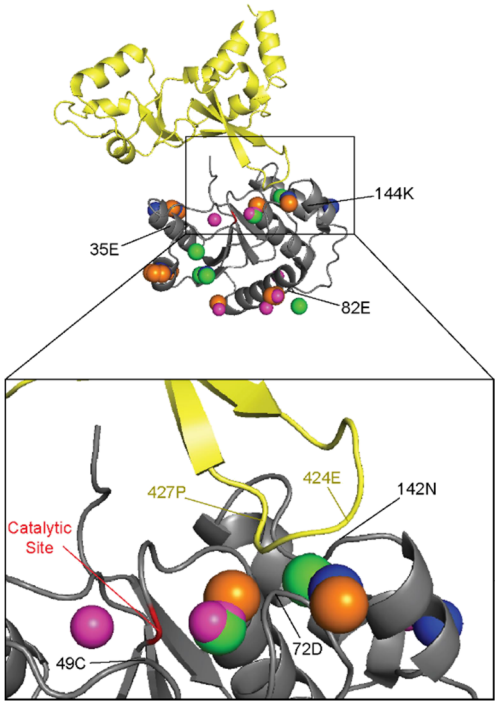

Figure 2. PRL-3 has numerous predicted metal binding sites. The crystal structure of PRL-3 in complex with the CBS domain of CNNM3 (PDB:5TSR) was analyzed using the metal ion-binding site prediction and modeling server (MIB2). The CBS domain (yellow) inserts a protruding loop into the active site of PRL-3 (gray). Predicted calcium, magnesium, manganese, and zinc binding sites are shown in orange, blue, green, and pink, respectively, with the PRL-3 catalytic site in red. Several predictions place metal ions directly in the CNNM interface or interacting with the nearby active site and WPD loop of PRL-3.

shown in Figure S2. We then sought to determine if these divalent metals could impact the thermal stability of PRL-3.

2.4. Calcium, Magnesium, and Manganese Ions Do Not Alter the Thermal Stability of PRL-3, but Zinc Ions Destabilize the Protein. We utilized label-free nano-differential scanning fluorometry (nanoDSF) to investigate the thermal stability of PRL-3 in the presence of the predicted metal-binding partners. The thermal stability of PRL-3 was evaluated in both a non-reducing buffer and a buffer supplemented with 0.5 mM DTT. The sole disulfide bond in PRL-3 forms between the catalytic residue (C104) and a non-catalytic cysteine (C49) near the active site. Consequently, high concentrations of reducing agents are necessary to enable PRL-3's enzymatic function in vitro. Under non-reducing conditions, the melting point of PRL-3 was determined to be 69.9 ± 0.6 °C, which decreased to 58.8 ± 0.2 °C in the presence of DTT. The addition of calcium, magnesium, and manganese salts at 200 and 400 μM concentrations exhibited no change in the thermal stability of PRL-3 under either redox state. However, $ZnCl_2$ significantly decreased the melting point of PRL-3 to 55.4 ± 0.7 and 50.87 ± 2 °C under non-reducing and reducing conditions, respectively, at 200 μM concentrations. We noted that doubling this $ZnCl_2$ concentration to 400 μM did not further destabilize the protein (Figure 4). The first derivative graphs used to calculate the T_m are shown in Figure S3. We also tested both $CaCl_2$ and $MgCl_2$ at 800 and 1200 μM but saw no significant change in the thermal stability of PRL-3 (Figure S4A). As expected, given our CD data, we

https://doi.org/10.1021/acsomega.3c04095
ACS Omega 2023, 8, 30578−30589

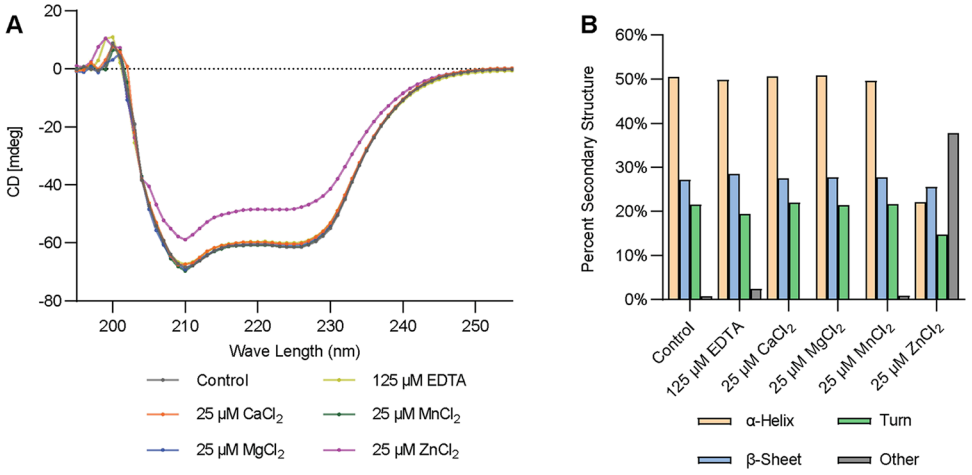

Figure 3. Secondary structure of PRL-3 is not altered by calcium, magnesium, or manganese but is disordered by zinc. (A) Circular dichroism (CD) spectra of PRL-3 in the presence or absence of the indicated metal salts, with 125 μM EDTA used as a negative control. (B) Raw CD data were interpreted using the BeStSel (Beta Structure Selection) platform to estimate the percent of PRL-3 in alpha-helix, beta-sheet, turn, or other/disordered secondary structural states after treatment with the indicated metal salts or EDTA.

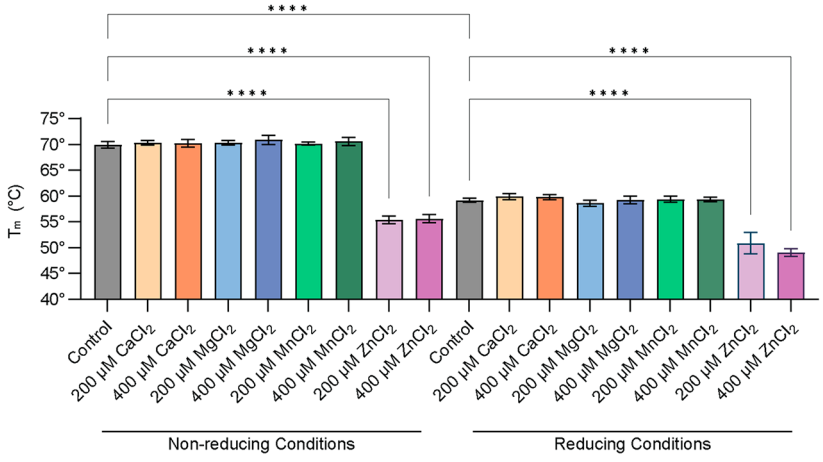

Figure 4. Calcium, magnesium, and manganese do not affect PRL-3 stability, but zinc has a destabilizing effect. The T_m (the temperature at which 50% of the protein is unfolded) of PRL-3 under non-reducing and reducing conditions in the presence or absence of the indicated metal salts. Error bars represent the standard deviation. The conditions were compared to the control using an ordinary one-way ANOVA analysis. ****$p < 0.0001$, comparing treatment with $ZnCl_2$ to the control and comparing controls under both redox states.

found that $ZnCl_2$ could destabilize PRL-3 in a dose-dependent manner under non-reducing conditions up until 50 μM, at which point higher concentrations did not compound any additional effect (Figure S4B).

Together, these data demonstrate that these divalent metal ions do not impact PRL-3 stability or structure, with the exception of zinc. Next, we sought to determine whether the enzymatic function of the protein could be modulated through a metal cofactor.

2.5. Enzymatic Activity of PRL-3 Is Insensitive to Divalent Metal Ions. We used the synthetic substrate 6,8-difluoro-4-methylumbelliferyl phosphate (DiFMUP) to evaluate the phosphatase activity of PRL-3.[38] This enzymatic assay typically uses a reaction buffer of 10 mM Tris−HCl (pH 7.5) and 15 mM NaCl with high concentrations of a reducing agent to maintain PRL-3 activity.[39] PRL-3 exhibited burst kinetics under these conditions, characterized by a single round of catalysis, followed by a slow steady-state activity, during which the phospho-cysteine intermediate was hydrolyzed to regenerate the active enzyme. We determined that a minimum of 0.5 μM of PRL-3 combined with 25 μM DiFMUP enabled quantification of both burst and steady-state enzymatic rates (Figure 5A), although PRL-3's enzymatic activity was modest under these conditions. The addition of 0.01% Triton-X into the reaction buffer doubled the intensity of both the burst-phase and steady-state enzymatic rates (Figures 5B and S5), and 5 mM tris(2-carboxyethyl) phosphine (TCEP) as a reducing agent maintained enzyme activity (Figure 5C). TCEP, known for its enhanced stability and reducing capacity compared to DTT,[40] was selected as an alternate reducing agent. The enhanced burst-phase enzymatic rate observed with the addition of Triton-X to the buffer is likely due to the detergent's prevention of surface absorption and stabilization of PRL-3's hydrophobic regions, increasing the fraction of active protein in each well. Figure 5D compares PRL-3's enzymatic activity between the original and optimized buffer conditions.

With the optimized assay conditions, we sought to determine the impact of Ca^{2+}, Mg^{2+}, Mn^{2+}, and Zn^{2+} on PRL-3's phosphatase activity. Metal salts were added into the

https://doi.org/10.1021/acsomega.3c04095
ACS Omega 2023, 8, 30578−30589

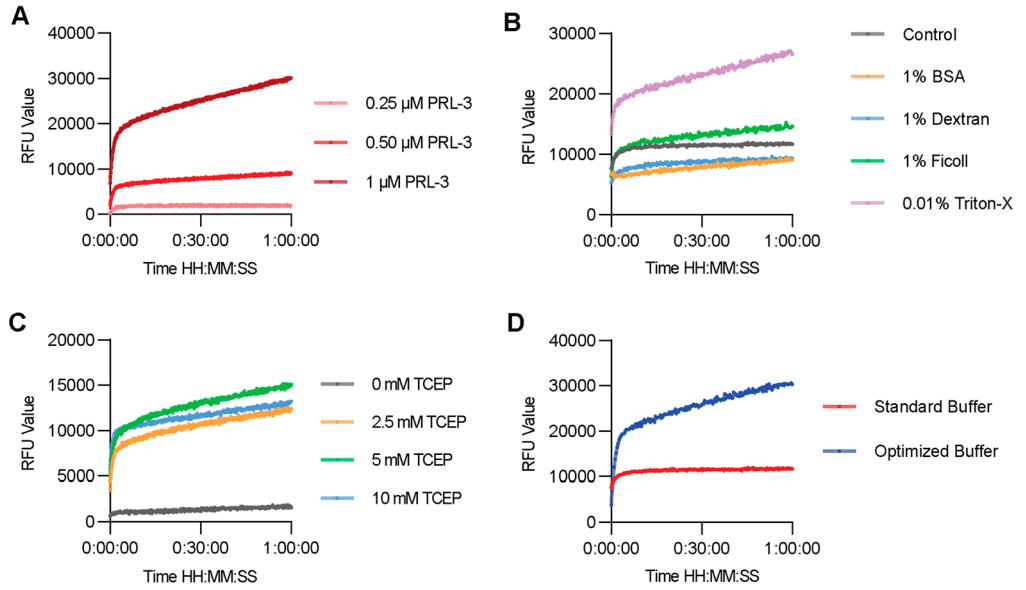

Figure 5. PRL-3 enzymatic activity against the synthetic substrate DiFMUP can be maximized using Triton-X and TCEP. (A) Mean relative fluorescence units (RFU) values produced over time with the indicated concentrations of purified PRL-3 protein incubated with an excess of DiFMUP in the standard assay buffer. (B) Adding 0.01% Triton-X to the standard assay buffer enhances the phosphatase activity of 0.5 μM PRL-3 compared to the standard assay buffer (control) and other crowding agents or detergents. (C) Indicated concentrations of tris (2-carboxyethyl) phosphine (TCEP) were tested as replacements for dithiothreitol (DTT) in the standard assay buffer (0 mM TCEP) to keep PRL-3 in a reduced, active state. (D) Comparison of the mean RFU values produced over time by 0.5 μM PRL-3 in an excess of DiFMUP, between standard buffer and "optimized" buffer containing 0.01% Triton-X and 5 mM TCEP.

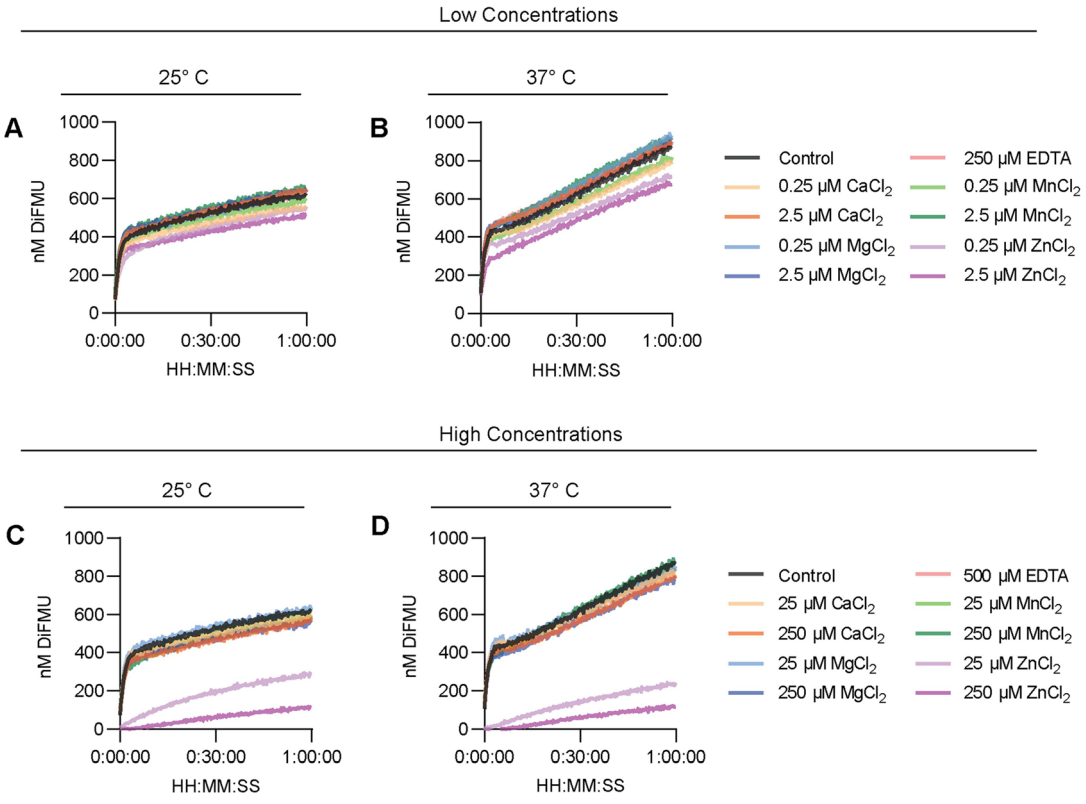

Figure 6. Divalent metals do not specifically impact the enzymatic activity of PRL-3. The mean amounts of DiFMU produced from the dephosphorylation of DiFMUP by PRL-3 over the course of an hour at 25 °C (A) and 37 °C (B) with low concentrations of metal salts or EDTA. (C, D) Mean amounts of DiFMU produced from the dephosphorylation of DiFMUP by PRL-3 over the course of an hour at 25 °C (C) and 37 °C (D) with high concentrations of metal salts or EDTA.

reaction buffer at the indicated concentrations, with EDTA as a control. The assays were conducted at 25 and 37 °C to examine potential temperature-dependent effects. During the burst phase, the rate of catalysis, measured by the formation of

https://doi.org/10.1021/acsomega.3c04095
ACS Omega 2023, 8, 30578−30589

dephosphorylated DiFMUP (DiFMU), was 39.2 ± 3.8 μM per hour at 25 °C and 53.4 ± 6.2 μM per hour at 37 °C, which decreased to 0.45 ± 0.01 μM per hour at 25 °C and 0.95 ± 0.04 μM per hour at 37 °C during the steady state, respectively. There was no observable difference in the rate of product formation at either temperature with any of the tested $CaCl_2$, $MgCl_2$, or $MnCl_2$ concentrations (Figure 6). Additionally, magnesium-ATP, the prevalent form of magnesium inside the cell, also had no impact on the enzymatic activity of PRL-3 (Figure S6). Individual burst-phase and steady-state calculations are shown in Figure S7. As anticipated, $ZnCl_2$ inhibited PRL-3's enzymatic activity, consistent with its effects on other protein phosphatases.[31] Zinc ions can have a non-specific inhibitory and destabilizing effect on many proteins through interactions with cysteine and histidine residues. The high concentration of reducing agents used in this assay would allow zinc ions to bind fully reduced thiol groups of the catalytic cysteine or others scattered throughout the structure.[41] Interestingly, $ZnCl_2$ concentrations lower than 25 μM did not impact the steady-state enzymatic rate of PRL-3 at 25 °C, suggesting that this inhibition only occurs at non-physiological concentrations of zinc (Figure S7B). These data indicate that these metal ions do not impact PRL-3's phosphatase activity in vitro, with the exception of high zinc concentrations. After dephosphorylating a substrate, PRL-3 must hydrolyze its phospho-cysteine to return to an active state, where it can either dephosphorylate a new substrate or participate in CNNM binding. We next sought to determine if the divalent metals had any impact on the stability of PRL-3's phospho-cysteine intermediate, as this could provide a potential mechanism by which the PRL:CNNM interaction to serve as a direct sensor of intracellular metal concentrations.

2.6. Stability of the PRL-3 Phospho-Cysteine Intermediate Is Not Impacted by Calcium, Magnesium, or Manganese Ions. We used Phos-Tag gel electrophoresis to determine if the metals ions could accelerate the hydrolysis of the PRL-3 phospho-cysteine intermediate. When incubated with an equimolar DiFMUP substrate, the phosphorylation of PRL-3 increased over time, reaching approximately 6% of PRL-3 at 1 min, 22% at 2.5 min, and 61% at 15 min. Saturation of the intermediate state was achieved and maintained between 15 and 45 min, with 83% of PRL-3 existing in the intermediate form at the 45-minute mark and remaining phosphorylated in subsequent time points (Figure S8). Next, equimolar PRL-3 and DiFMUP (2.5 μM) were incubated with 250 μM of the metal salts, and reactions were stopped at 5 min to visualize the burst phase and 45 min to visualize the steady-state rate (Figure 7A). Quantitative analysis revealed no significant difference in the percentage of phosphorylated PRL-3 at either time when incubated with $CaCl_2$, $MgCl_2$, or $MnCl_2$ (Figure 7B). $ZnCl_2$ inhibited the formation of the enzymatic intermediate, potentially due to the denaturation of the enzyme or through direct non-specific interactions within the active site, thereby disrupting enzymatic activity. Our findings demonstrate that calcium, magnesium, and manganese ions do not alter the stability, structure, or enzymatic activity of PRL-3. We next tested the ability of these metals to directly disrupt PRL:CNNM interaction, which would serve as a convenient mechanism for PRL-3 to function as a sensor of intracellular metal concentrations.

2.7. Divalent Metal Ions Do Not Directly Modulate Interactions between PRL-3 and the CBS Domain. To

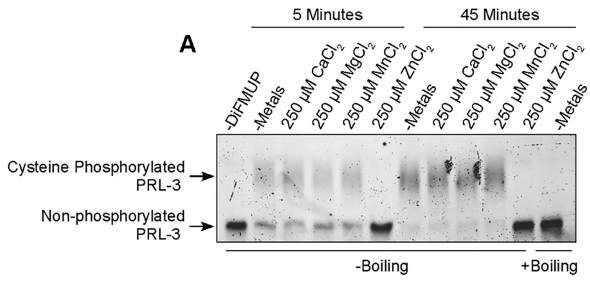

B

Normalization to Lane 1		
Lane	Condition:	Percent Phosphorylated
1	No DiFMUP	0.0
2	No Metal, 5 min	50.9
3	$CaCl_2$, 5 min	56.6
4	$MgCl_2$, 5 min	55.9
5	$MnCl_2$, 5 min	50.1
6	$ZnCl_2$, 5 min	1.5
7	No Metal, 45 min	80.3
8	$CaCl_2$, 45 min	81.2
9	$MgCl_2$, 45 min	77.5
10	$MnCl_2$, 45 min	77.4
11	$ZnCl_2$, 45 min	1.1

Figure 7. Divalent metals do not alter the formation or hydrolysis of the PRL-3 phospho-cysteine intermediate. (A) Recombinant PRL-3 was incubated with DiFMUP and the metal salts for the designated time period. The samples were then analyzed using Phos-Tag acrylamide and gel electrophoresis to separate the non-phosphorylated PRL-3 (bottom bands) from the phospho-cysteine intermediate form (top bands). Cysteine phosphorylation is sensitive to boiling, as demonstrated in the last lane as a control. (B) Band quantifications of each condition to estimate the percent of PRL-3 in the phospho-cysteine intermediate state normalized to the no DiFMUP control in lane 1.

determine if the PRL-3:CNNM interaction is disrupted in the presence of metal ions, we utilized an in vitro pulldown assay. The CBS domain of CNNM protein binds tightly into the active site of PRL-3. Purified HA-CBS was therefore loaded onto anti-HA magnetic beads and then mixed with purified PRL-3 to determine the impact of metals on PRL-3:CNNM binding. Figure 8A demonstrates validation of the antibodies. Our findings indicate that the presence of $CaCl_2$, $MgCl_2$, or $MnCl_2$ has no impact on the ability of PRL-3 to bind with the CNNM3 CBS domain (Figure 8B). However, $ZnCl_2$ decreased the interaction between PRL-3 and HA-CBS. Although our prior data suggest that inhibitory effects of zinc ions on PRL-3 are most likely due to non-specific destabilization of the protein, our current experiments cannot entirely dismiss the possibility that zinc ions directly inhibit the PRL-3:CBS interaction. Additional studies are necessary to define zinc's mechanism of inhibition.

3. DISCUSSION

In this study, we investigated the influence of divalent metals on the activity and binding functions of PRL-3. Given its role in regulating CNNM function and the potential interaction with the TPRM7 ion channel via CNNM, we hypothesized that PRL-3 could act as a direct sensor of intracellular metal concentrations for cellular homeostasis. While in silico modeling predicted several metal binding sites near the PRL-

https://doi.org/10.1021/acsomega.3c04095
ACS Omega 2023, 8, 30578−30589

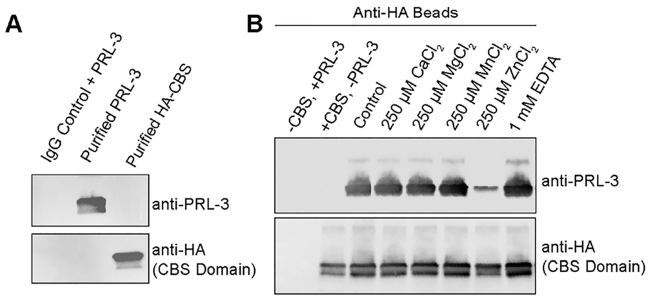

Figure 8. Calcium, magnesium, and manganese have no impact on the ability of PRL-3 to bind the CBS domain, while zinc destabilizes the interaction. (A) Experimental control showing the rabbit IgG isotype control incubated with PRL-3 does not immunoprecipitate protein, and verification of antibody sensitivities against purified PRL-3 and HA-CBS. (B) PRL-3 was incubated with the metal salts or EDTA before being combined with magnetic beads loaded with purified HA-CBS protein. The ability of PRL-3 to bind the CBS domain was analyzed by Western blot.

3 active site, our experimental data demonstrated that PRL-3 function is insensitive to calcium, magnesium, and manganese.

However, we observed that Zn^{2+} could impact PRL-3 activity and CNNM binding, although we believe that this is a non-specific interaction. In the cellular context, zinc is primarily bound to proteins, and the intracellular concentrations of free zinc are maintained in the 600 pM−1 nM range.[42,43] Numerous phosphatases can be inhibited by zinc, though the mechanism of inhibition is a topic of debate. Some studies report that high zinc concentrations are required to see enzymatic inhibition; for example, protein phosphatase 2A activity is inhibited with 10 μM zinc. Non-physiological zinc concentrations make it challenging to discern if the inhibitory effects are due to inhibition of the catalytic site or overall destabilization of the protein.[44] In contrast, the activity of PTP1B can be inhibited by picomolar zinc concentrations, suggesting that zinc can specifically interact with the active site to inhibit the protein.[45] In the case of PRL-3, concentrations as high as 25 μM were needed to inhibit phosphatase activity at 25 °C despite lower concentrations having destabilizing effects, as apparent through our CD and thermal stability analysis. Although previous studies suggested that Zn^{2+} can inhibit the PRL:CNNM interaction at very high (10 mM) concentrations,[46] we found that concentrations as low as 5 μM disorder the secondary structure of PRL-3, and concentrations as low as 12.5 μM decreased the T_m by 5 °C (Figures S2 and S4). These data suggest that any inhibitory effect of Zn^{2+} on PRL-3 is likely due to the non-specific destabilization of the protein. These observations suggest that physiological zinc ion concentrations would not directly impact PRL-3 activity. Although divalent metals did not affect the function of purified PRL-3 protein, it remains possible that they could regulate other aspects of PRL-3 biology within the cell. Fluctuations in intracellular metal concentrations can influence transcription,[47] substrate availability,[48] intracellular pH,[49] and trafficking,[50] all of which may significantly affect PRL-3 inside the cell.

The PRL:CNMM interaction is of significant interest, given the importance of CNNM binding to the ability of PRL-3 to drive metastatic phenotypes. The most well-established regulator of the PRL:CNNM interaction is the cysteine phosphorylation of PRLs. The active site cysteine undergoes rapid phosphorylation as part of PRL enzymatic activity. Unlike most phosphatases, PRLs exhibit very slow hydrolysis of their phosphorylated intermediate state, which can persist for an hour or more.[26] PRLs cannot bind CNNM proteins in this phospho-cysteine intermediate form.[15,23] Our data confirm that the phospho-cysteine intermediate inhibits interactions between the CBS domain and PRL-3 and that the CBS domain can inhibit PRL-3 phosphatase activity in vitro (Figure S9). Considering our finding that PRL-3 has a broad substrate specificity, with activity against many non-protein substrates, it is likely that PRL-3 predominantly exists in a phospho-cysteine state in the cell, hindering its interaction with CNNM. Notably, PRL-1 and 2 isolated from normal mouse tissues were found to be predominantly cysteine phosphorylated.[23] However, whether PRL-3 is in an intermediate or active state in cancer cells and the extent of association with CNNMs throughout cancer progression is still unknown. Understanding the regulation of the phospho-cysteine intermediate of PRL-3 by other proteins or cofactors in normal and cancer cells could provide insights into PRL-3:CNNM binding. Characterization of the proteins and mechanisms responsible for regulating the PRL-3:CNNM interaction will expand our toolkit for disrupting the oncogenic activity of PRL-3.

4. CONCLUSIONS

In this investigation, we screened the broad enzymatic activity of the PRL family against a variety of cellular moieties and found that PRL-3 could dephosphorylate nucleotides, amino acids, NADPH, and inositol lipids with various degrees of activity toward each. Our in silico predictions found numerous metal binding sites on PRL-3, with many predictions occurring within the PRL:CNNM interface. We used a series of biophysical analyses to determine that the stability, structure, enzymatic activity, and CNNM binding capacity of PRL-3 are unaffected by calcium, magnesium, and manganese ions in vitro, while zinc ions have a non-specific destabilizing effect. We determine that PRL-3 is not directly sensitive to these metals in vitro, highlighting the need for further investigations to understand the regulators of the PRL:CNNM interaction within the cell to define this oncogenic complex as a therapeutic target.

5. METHODS

5.1. Plasmids and Cloning. We used the pSKB3 bacterial expression vector to express and purify recombinant PRL and HA-CBS domain proteins. The pSKB3 plasmid is a derivative of the pET-28b vector, replacing the thrombin cleavage site with a tobacco etch virus (TEV) protease cleavage site and was a gift from Dr. Konstantin Korotkov at the University of Kentucky.[51] Full-length human PRL-(1, 2, or 3) cDNA or HA-CBS was cloned into the pSKB3 vector using the NheI and XhoI restriction sites via T4 ligase.[52] The HA-CBS construct was obtained from a full-length CNNM3 CBS domain-pair (residues Y301-D451, RefSeq NM_017623.5) gBlock Gene Fragment (IDT), with a human influenza hemagglutinin epitope tag fused to the N-terminus.

5.2. Protein Purification. The previously described pSKB3-PRL-(1,2,3) and pSKB3-HA-CBS plasmids were transformed into One-Shot BL21 Star DE3 Chemically Competent *E. coli* (Invitrogen, C601003). The transformed bacteria were incubated with shaking at 37 °C in Lennox LB (Millipore Sigma, L3022) with appropriate antibiotic selection, and growth was monitored by measuring the optical density of the culture (OD_{600}). When an OD_{600} of 0.6 was reached, the

https://doi.org/10.1021/acsomega.3c04095
ACS Omega 2023, 8, 30578−30589

flasks were placed on ice, and protein expression was induced by adding 0.5 mM IPTG (Fisher Scientific, BP175510) and then incubated with shaking for 16 h at 16 °C. The bacterial cells were then pelleted at 10,000 RCF at 4 °C using a Sorvall LYNX 4000 Superspeed Centrifuge (Thermo Scientific, 75,006,580). The bacteria pellets were resuspended in 10 mL of lysis buffer [300 mM NaCl (VWR BDH9286), 20 mM Tris pH 7.5, 10 mM imidazole pH 8.0 (Sigma-Aldrich I2399), 1:1000 protease inhibitor cocktail (Sigma-Aldrich P8465) per gram of cell pellet]. To ensure adequate lysis, the cells were lysed by passing through a microfluidizer (Avestin, EmulsiFlex-C5) twice. Bacterial debris was pelleted at 38,000 RCF for 50 min at 4 °C. The collected supernatant was passed through Econo-Pac Chromatography Columns (Bio-Rad, 7321010) loaded with Ni-NTA resin (VWR, 786-940). PRL-3 or HA-CBS proteins were eluted from the resin with 2 mL elution buffer (300 mM NaCl, 20 mM Tris pH 7.5, and 250 mM Imidazole pH 8.0). The N-terminal 6xHis-tag was then cleaved from the recombinant proteins using TEV protease (purified in a similar manner) and subjected to overnight dialysis by loading the sample into SnakeSkin Dialysis Tubing (Thermo Scientific, 68100) and dialyzing against 1 L of imidazole free buffer at 4 °C with stirring. The purified proteins were passed through a Ni-NTA resin to remove any uncleaved recombinant protein. Both PRL-3 and HA-CBS were further purified using a Superdex 200 Increase 10/300 GL column (GE, 28990944) on an ÄKTA purification system (GE Healthcare) with a 100 mM NaCl and 20 mM HEPES pH 7.5 (Fisher Scientific, BP310−100) buffer. The quality of the purification was verified by running the recombinant protein fractions on 4−20% Mini-PROTEAN TGX Stain-Free Gels (Bio-Rad 4568094) and visualizing the protein bands using the Stain-Free channel on a Chemidoc Touch Imaging System (Bio-Rad, 1708370). Stain-free imaging utilizes a proprietary compound that covalently modifies the tryptophan residues in the protein to generate a fluorescent signal that is visualized by UV excitation. The purified HA-CBS lacks tryptophan and cannot be visualized using Stain-Free technology. To visualize these bands, we utilized an in-house Coomassie staining protocol. Briefly, Brilliant Blue G (Millipore Sigma, B0770) was dissolved in 85% phosphoric acid ACS reagent (Thermo Scientific, 424040025) before being diluted in water. This reagent was then utilized following conventional Coomassie staining protocols.[53] A comparison of these visualization techniques and validation of the protein purity is shown in Figure S10. The fractions with the purest band patterns were then pooled, flash-frozen with liquid nitrogen, and stored at −80 °C.

5.3. Malachite Green Substrate Screen. A malachite green assay kit (R&D Systems, DY996) was used to quantify the release of inorganic phosphate produced when the PRL proteins were incubated with the potential substrates, following the "high-sensitivity" protocol according to the manufactures instructions. Purified PRL proteins were incubated in a reaction buffer containing 10 mM Tris−HCl (pH 7.5), 15 mM NaCl, 0.01% Triton-X, and 5 mM TCEP before analysis to ensure the reduction of the enzymatic active site. The PRLs were suspended in the same buffer at a concentration of 2.5 μM, and the substrates were added at 50 μM concentrations. Parallel samples were prepared without PRL proteins for background subtraction for each compound. The PRL/substrate mixtures and controls were incubated for 1.5 h at 37 °C with gentle rotation. After incubation, the reactions were stopped by adding 3 M sulfuric acid, and samples were processed according to the manufacturer's instructions. Samples were plated in black 96-well plates in triplicates with individual substrates wells for background subtraction. The sample absorbance at 620 nm was measured using a Synergy LX Multi-Mode Reader (BioTek/Agilent). The calculated absorbance values were correlated to a concentration of inorganic phosphate derived from a standards curve generated using the kit manufacturer's instructions. The assay was performed twice for PRL-3 with pooled values and once for PRL-1 and PRL-2. The results were analyzed using a one-way ANOVA analysis in GraphPad Prism 9 with p-values <0.05 considered significant.

The following compounds were utilized in this assay: DiFMUP, 6,8-difluoro-4-methylumbelliferyl phosphate (Thermo Fisher, D6567); pNPP, p-nitrophenyl phosphate, disodium salt (NEB, P0757S); DDAOP, 9H-(1,3-dichloro-9, 9-dimethylacridin-2-ona-7-yl)-phosphate (Bimol, ABD-11629); phospho-serine, O-phospho-L-serine (Cayman Chemical, 16151); phospho-threonine, O-phospho-L-threonine (Cayman Chemical, 35057); phospho-tyrosine, O-phospho-L-tyrosine (Cayman Chemical, 23064); Mg-ATP, equimolar mix of $MgCl_2$ and ATP; ATP, adenosine 5′-triphosphate (Gold Biotechnology, A-081-1); ADP, adenosine 5′-diphosphate (USBio, 10,490); AMP, adenosine 5-monophosphate (CalBioChem, 118110); cAMP, 3′-5′-cyclic adenosine monophosphate (Sigma, A6885); Mg-GTP equimolar mix of $MgCl_2$ and GTP; GTP, guanosine 5′-triphosphate (Sigma, G-8877); GDP, guanosine 5′-diphosphate (Sigma, G-7127); GMP, guanosine 5′-monophosphate (Cayman Chemical, 16957); cGMP, 3′-5′-cyclic guanosine monophosphate (Sigma, G6129); CTP, cytosine 5′-triphosphate (Sigma, C-1506); UTP, uridine 5′-triphosphate (Sigma, U-6625); NADH, β-nicotinamide adenine dinucleotide (Sigma-Aldrich, N7004); NADPH, β-nicotinamide adenine dinucleotide 2′-phosphate (Sigma-Aldrich, N1630); G6P, glucose 6-phosphate (Sigma-Aldrich, G7879); F6P, fructose 6-phosphate (Sigma-Aldrich, F3627); F1,6P, fructose 1,6-bisphosphate (Sigma-Aldrich, F6803); GA3P, glyceraldehyde 3-phosphate (Sigma-Aldrich, G5251); 3PG, 3-phosphoglycerate (Sigma, p8877); 16:0 PA, 1,2-dipalmitoyl-sn-glycero-3-phosphate (sodium salt) (Avanti, 830855); PI, phosphatidylinositol diC8, (Echelon, P-0008); IP6, D-myo-inositol-1,2,3,4,5,6-hexaphosphate (Cayman Chemical, 10008415); PI(3)P, phosphatidylinositol 3-phosphate diC8 (Echelon, P-3008); PI(4)P, phosphatidylinositol 4-phosphate diC8 (Echelon, P-4008); PI(5)P, phosphatidylinositol 5-phosphate diC8 (Echelon, P-5008); PI(3,4)P_2, phosphatidylinositol 3,4-bisphosphate diC8 (Echelon, P-3408); PI(3,5)P_2, phosphatidylinositol 3,5-bisphosphate diC8 (Echelon, P-3508); PI(4,5)P_2, phosphatidylinositol 4,5-bisphosphate diC8 (Echelon, P-4508); and PI(3,4,5)P_3, phosphatidylinositol 3,4,5-trisphosphate diC8 (Echelon, P-3908).

5.4. In Silico Metal Binding Predictions. A metal binding site prediction tool analyzed the crystal structure of PRL-3 in complex with the CBS domain of CNNM3 or PRL-3 alone using PDB: 5TSR[16] and 1V3A[37] structures, respectively. The MIB2 (metal ion-binding site prediction and modeling server) was used to analyze the structure and predict potential binding sites for calcium, magnesium, manganese, and zinc.[54] The server utilizes PDB templates of known metal binding sites and applies these templates to the structure of interest to screen for similarities and score the predictions. The top five predictions with the highest score for each metal on either structure are summarized in Table S1. Molecular figures were

https://doi.org/10.1021/acsomega.3c04095
ACS Omega 2023, 8, 30578−30589

created using the PyMOL Molecular Graphics System, Version 2.5.4, Schrödinger, LLC.

5.5. CD Spectroscopy and Interpretation. Purified PRL-3 was diluted with ddH_2O to achieve 25 μM PRL-3 samples (1 mM NaCl and 200 μM HEPES pH 7.5). Samples were prepared in the presence or absence of the metal salts at 5 and 25 μM concentrations or 125 μM EDTA. 400 μL of the samples was loaded into quartz cuvettes with a 1 nm path length (Strana Cell, 21-I-1) and analyzed using a Jasco J-810 Circular Dichroism Spectropolarimeter. The 200−250 nm far-UV spectra were recorded through 1 nm intervals at 25 °C. Each sample containing protein was normalized to the respective buffer control. The spectra were collected through five replicates and averaged for each analysis. The assay was repeated twice for each condition using purified PRL-3 from two independent rounds of protein purification. The generated CD spectra were then interpreted using the BeStSel (Beta Structure Selection) platform to estimate the percent secondary structures of the samples.[55] The calculated curve fittings had reported NRMSD values <0.025.

5.6. Thermal Stability Analysis Using Differential Scanning Fluorimetry. We utilized dye/label-free differential scanning fluorimetry (nanoDSF) to determine the thermal stability of PRL-3 in the presence of metal salts. We used a Tycho NT.6 system (Nanotemper), which measures the intrinsic fluorescence of tryptophan and tyrosine residues and quantifies the change in this ratio over a gradual increase in temperature. Tycho NT.6 Capillaries were loaded with samples of 40 μM PRL-3 (resuspended in 100 mM NaCl and 20 mM HEPES pH 7.5) with or without 0.5 mM DTT (Thermo Scientific, R0861) and the metal salts or EDTA (Armesco Life Science, E522). The loaded capillaries were placed into the Tycho NT.6 and subjected to a thermal ramp from 35 to 95 °C. Data output calculated by the Tycho Software includes the inflection temperature (T_i), initial ratio (350 nm/330 nm at 35 °C), Δ ratio (between 95 and 35 °C), and sample brightness. The T_i values (also referred to as the melting temperature or T_m) represent the temperature at which half of the protein population is in an unfolded state. Samples were preincubated with calcium chloride (VWR, 97062-590), magnesium chloride (VWR, 12315-A1), manganese chloride (ChemCruz, sc-358,271), or zinc chloride (Thermo Scientific, A16281.22) in the sample buffers (±DTT) for 30 min before the analysis. The assay was performed twice with three technical replicates and utilized protein from two independent rounds of purification. The T_m values from each assay were pooled and analyzed using a one-way ANOVA analysis in GraphPad Prism 9 with p-values <0.05 considered significant.

5.7. Optimizing PRL-3 Enzymatic Reaction Buffer. The synthetic substrate 6,8-difluoro-4-methylumbelliferyl (DiFMUP) was used to quantify PRL-3 enzymatic activity using the EnzChek Phosphatase Assay Kit (Thermo Scientific, E12020). Upon hydrolysis of the phosphate group from DiFMUP, the 6,8-difluoro-7-hydroxy-4-methylcoumarin (DiFMU) product can be quantified with a plate reader to measure fluorescence. This synthetic substrate is ideal for PRL-3 as it allows for the observation of both the burst and steady-state enzymatic rates by quantifying the dephosphorylated fluorescent substrate rather than quantifying the release of inorganic phosphate, which would neglect the burst-phase enzymatic rate. PRL-3 was incubated with an excess of DiFMUP (21 μM) with RFUs reported over time. PRL-3 was suspended in a buffer containing 10 mM Tris−HCl (pH 7.5), 15 mM NaCl and 20 mM DTT or various TCEP concentrations (Thermo Scientific, 77,720). Crowding agents or detergents, including bovine serum albumin (Fisher Bioreagents, BP9706-100), Dextran T500 (Pharmacia Biotech, 12-0320-01), Ficoll-Plaque Premium 1.073 (VWR, 17-5446-52), and Triton X-100 (Sigma, X100) were added into the reaction buffer for pre-incubation with PRL-3 at the reported concentrations. PRL-3 was pre-incubated in the reaction buffers for 30 min before experimental analysis to ensure complete reduction. One technical limitation to these investigations is the ability to separate the quick burst-phase from the slow steady-state enzymatic rates.[26] Black 384 well low retention plates (Corning, 3575) were preloaded with PRL-3 resuspended in reaction buffer before DiFMUP was added to overcome this. An Integra ViaFlow 96-channel pipette robot was then used to inject and mix DiFMUP into the reaction wells to a final volume of 25 μL to ensure the simultaneous initiation of the enzymatic reaction across the plate. The plate was then immediately placed on a BioTek Cytation 7 machine using the sweep function to rapidly read all wells at Ex:360/10 Em:450/10 over an hour at 25 °C. Using this method, we captured over 50 data points per well occurring within the burst-phase portion of the reactions (depending on the scale of the analysis). Each well containing PRL-3 was paired with a control well containing the corresponding buffer of each condition and DiFMUP to be used for background subtraction at each time point. The results were analyzed by averaging the RFU values between 6 and 12 technical replicate wells. The results for optimal PRL-3 concentration, detergent or additive concentration, and reducing agent concentration were performed as independent experiments before the analysis with the final optimized buffer.

5.8. PRL-3 Enzymatic Activity in the Presence of Metal Salts. A similar methodology was used to determine how metal salts impact PRL-3 enzymatic activity. Sample wells were loaded with 0.5 μM PRL-3 in the optimized buffer (10 mM Tris−HCl (pH 7.5), 15 mM NaCl, 0.01% Triton-X, and 5 mM TCEP) with the addition of either the metal salts or EDTA. Reactions were initiated and read similarly using 25 μM DiFMUP in 25 μL reaction volumes with 12 technical replicates for each condition. The assay was performed at 25 °C and then repeated at 37 °C. To correlate the RFU value readouts to concentrations of the product being formed, we used the dephosphorylated standard (DiFMU) provided in the EnzChek Phosphatase Assay Kit to generate a standards curve using multiple concentrations ranging from 1 to 3000 nM and used this to estimate product formation. This assay was repeated twice with independently purified protein samples, and the results were pooled together to generate the final data set. The amount of product formation was plotted as a function over time. Comparative to lone magnesium chloride, an equimolar solution of $MgCl_2$, and adenosine-5′-triphosphate disodium trihydrate (ATP), Ultra-Pure (Gold Biotechnology, A-081-1) was used to replicate intracellular magnesium-ATP conditions. In addition to testing enzymatic activity with magnesium-ATP, an additional reaction sample of PRL-3 with ATP alone was initiated and read under the same experimental conditions. The assay was also repeated with various concentrations of purified HA-CBS domain protein as an inhibitor of PRL-3 enzymatic activity. The burst and steady-state enzymatic rates were separated, and we used the Excel Solver Function to curve fit the slopes to determine the rate of

https://doi.org/10.1021/acsomega.3c04095
ACS Omega 2023, 8, 30578−30589

product formation.[56] The enzymatic rates were compared using a one-way ANOVA analysis in GraphPad Prism 9 with p-values <0.05 considered significant.

5.9. Phospho-Cysteine Stability Determination via Phos-Tag Gel Electrophoresis. Purified PRL-3 at a concentration of 2.5 μM was preincubated in the optimized reaction buffer with the metal salts for 30 min before equimolar DiFMUP was added. The reactions were allowed to proceed for the allotted time before being stopped by adding Laemmli buffer (Biorad, 161-0737) with 2-mercaptoethanol (Fisher Scientific, 03446I-100). Samples were then separated via gel electrophoresis using 1 mm 10% Stain-Free Acrylamide (Bio-Rad, 1610182) gels containing 25 μM Phos-Tag Acrylamide (Wako Chemicals, AAL-107) and 50 μM manganese chloride to activate the compound. Protein separation was performed using a Mini-PROTEAN Tetra Cell (Bio-Rad, 1658005EDU) gel electrophoresis tank. Protein bands were then visualized using the Stain-Free function on a ChemiDoc Touch Imaging System. When added to the resolving solution of acrylamide gels, the Phos-Tag Acrylamide retards the migration of phosphorylated proteins, allowing the distinction between phosphorylated and non-phosphorylated protein forms. Upon incubation with DiFMUP, the PRL-3 phospho-cysteine intermediate can be readily identified as a band smear that migrates slower than the naïve protein. Relative band intensities were then quantified using Fiji ImageJ2 and normalized to the no DiFMUP control.[57] Cysteine phosphorylation has the unique property of being susceptible to removal by boiling, and this was included as an experimental control. Phosphate groups on serine/threonine form stable phosphodiester bonds with the amino acid side chains and are more resistant to heating than cysteine phosphorylation, a phosphothioester bond.[15]

5.10. PRL-3 and HA-CBS In Vitro Binding Assay. Purified HA-CBS was incubated with HA-Tag (C29F4) rabbit mAb magnetic bead conjugate (Cell Signaling, 11846S, Lot #9) at a concentration of 2.5 μM for 1 hour at room temperature suspended in immunoprecipitation (IP) buffer containing 25 mM Tris−HCl pH 7.4, 150 mM NaCl, 1% NP-40 (Abcam, ab142227), and 5% glycerol (VWR, 0854). Equimolar PRL-3 was incubated in separate tubes containing IP buffer and 1 mM TCEP to ensure the protein was reduced. PRL-3 was incubated with 250 μM of the metal salts, 1 mM EDTA, or DiFMUP for 30 min before the assay. The HA-CBS loaded beads were then combined with the PRL-3 samples and incubated for 1 h at room temperature with rotation. The immuno-complexes were separated using a magnetic rack and washed three times with excess IP buffer. The immuno-complexes were then eluted with 50 μL of 4× Laemmli sample buffer and 2-mercaptoethanol and boiled at 95 °C for 5 min. As an experimental control, Protein A magnetic beads (Cell Signaling, 73778S) were incubated with an excess of rabbit (DA1E) mAb IgG XP (R) (Cell Signaling, 3900S, Lot #37) for 1 h at room temperature before being washed three times with IP buffer. PRL-3 prepared in a manner similar to that mentioned above was incubated with the isotype control beads for an hour before being washed three times with IP buffer to validate that there was no non-specific binding occurring. The control complexes were eluted in the same manner as mentioned above. Purified HA-CBS, PRL-3, and the isotype control sample were diluted into Laemmli buffer for analysis by gel electrophoresis and Western blotting as additional experimental controls.

5.11. Gel Electrophoresis and Western Blotting. Samples and experimental controls generated from the in vitro binding assay (above) were then prepared for gel electrophoresis by loading 5% of the elution into 4−20% Mini-PROTEAN TGX Stain-Free Protein Gels and ran at 150 V for 55 min. The protein gels were then transferred to an Immun-Blot PVDF Membrane (Bio-Rad, 1620255) using a Trans-Blot Turbo Transfer System (Bio-Rad, 1704150). The membranes were then blocked in 5% milk in 0.1% TBST for 1 h. Primary antibodies were then applied using either HA-Tag (6E2) Mouse mAb (Cell Signaling, Cat #2367, Lot #5) or anti-Human/Mouse/Rat PRL-3 Antibody (R&D Systems, MAB3219, Lot. WXH0421111) both at 1:1000 concentrations suspended in 5% milk in 0.1% TBST overnight at 4 °C with agitation. Following incubation with the primary antibody, blots were washed three times with 0.1% TBST for 5 min. Blots were then incubated with a secondary HRP-conjugated anti-mouse IgG antibody (Cell Signaling, 7076P2, Lot. 38) at 1:2500 for 1 h. Blots were again washed three times with 0.1% TBST for 5 min. The bands were visualized using the Clarity Western ECL Substrate Kit (Bio-Rad, 1705060) and the chemiluminescence channel on the ChemiDoc Touch Imaging System. The immunoblots were stripped by incubating in Restore PLUS Western Blot Stripping Buffer (Thermo Fisher, 46430) for 10 min and then re-blocked with 5% milk in 0.1% TBST before incubation with different primary antibodies.

■ ASSOCIATED CONTENT

Supporting Information

The Supporting Information is available free of charge at https://pubs.acs.org/doi/10.1021/acsomega.3c04095.

PRL-1 and PRL-2 dephosphorylate similar substrates as PRL-3, summary of the predicted metal binding sites, zinc disorders PRL-3 secondary structure in a dose-dependent manner, zinc altering the first derivative 330 nm and 350 nm wavelength signals of PRL-3 during the thermal ramp, figure showing that high calcium and magnesium concentrations do not affect PRL-3 stability, while $ZnCl_2$ destabilizes the protein, figure showing that lower concentrations of crowding agents and detergents have less impact in the DiFMUP phosphatase assay, figure showing that enzymatic activity of PRL-3 is not altered by the presence of magnesium-ATP or ATP alone, burst-phase and steady-state enzymatic rates of PRL-3, amount of PRL-3 in a phospho-cysteine intermediate state that can be quantified using the Phos-Tag gel system, CBS binding inhibiting PRL-3 enzymatic activity, and the PRL-3 enzymatic intermediate inhibits CBS binding, and successful purification of recombinant PRL-3 and HA-CBS from bacteria (PDF)

■ AUTHOR INFORMATION

Corresponding Author

Jessica S. Blackburn − *Department of Cellular & Molecular Biochemistry, University of Kentucky, Lexington, Kentucky 40536, United States; Markey Cancer Center at the University of Kentucky, Lexington, Kentucky 40536, United States;* orcid.org/0000-0001-9464-3784; Email: jsblackburn@uky.edu

https://doi.org/10.1021/acsomega.3c04095
ACS Omega 2023, 8, 30578−30589

Authors

Jeffery T. Jolly − *Department of Cellular & Molecular Biochemistry, University of Kentucky, Lexington, Kentucky 40536, United States; Markey Cancer Center at the University of Kentucky, Lexington, Kentucky 40536, United States;* orcid.org/0000-0002-6748-3591

Ty C. Cheatham − *Department of Cellular & Molecular Biochemistry, University of Kentucky, Lexington, Kentucky 40536, United States; Markey Cancer Center at the University of Kentucky, Lexington, Kentucky 40536, United States*

Complete contact information is available at: https://pubs.acs.org/10.1021/acsomega.3c04095

Notes

The authors declare no competing financial interest.

■ ACKNOWLEDGMENTS

We want to thank Dr. Konstantin Korotkov and Dr. Catherine Chaton for their help with protein purification, nanoDSF, and general technical assistance, as well as Dr. Martin Chow and Dr. David Rodgers for their help with CD experiments and project input. In addition, we want to thank Dr. Young-Sam Lee for providing the metabolites for the enzymatic screen and Dr. Pete Spielmann for his assistance and advice regarding the project. Finally, we thank Dr. Kalle Gehring for his input and for sharing his PRL-3 structure and function expertise. This work was funded by NCIR37CA227656 and NIH DP2CA228043 to J.S.B.

■ REFERENCES

(1) Zeng, Q.; Hong, W.; Tan, Y. H. Mouse PRL-2 and PRL-3, two potentially prenylated protein tyrosine phosphatases homologous to PRL-1. *Biochem. Biophys. Res. Commun.* **1998**, *244*, 421−427.

(2) Saha, S.; Bardelli, A.; Buckhaults, P.; Velculescu, V. E.; Rago, C.; St Croix, B.; Romans, K. E.; Choti, M. A.; Lengauer, C.; Kinzler, K. W.; et al. A phosphatase associated with metastasis of colorectal cancer. *Science* **2001**, *294*, 1343−1346.

(3) Wang, L.; Peng, L.; Dong, B.; Kong, L.; Meng, L.; Yan, L.; Xie, Y.; Shou, C. Overexpression of phosphatase of regenerating liver-3 in breast cancer: association with a poor clinical outcome. *Ann. Oncol.* **2006**, *17*, 1517−1522.

(4) Li, Z.-R.; Wang, Z.; Zhu, B.-H.; He, Y.-L.; Peng, J.-S.; Cai, S.-R.; Ma, J.-P.; Zhan, W.-H. Association of Tyrosine PRL-3 Phosphatase Protein Expression with Peritoneal Metastasis of Gastric Carcinoma and Prognosis. *Surg. Today* **2007**, *37*, 646−651.

(5) Mayinuer, A.; Yasen, M.; Mogushi, K.; Obulhasim, G.; Xieraili, M.; Aihara, A.; Tanaka, S.; Mizushima, H.; Tanaka, H.; Arii, S. Upregulation of Protein Tyrosine Phosphatase Type IVA Member 3 (PTP4A3/PRL-3) is Associated with Tumor Differentiation and a Poor Prognosis in Human Hepatocellular Carcinoma. *Ann. Surg. Oncol.* **2013**, *20*, 305−317.

(6) Ren, T.; Jiang, B.; Xing, X.; Dong, B.; Peng, L.; Meng, L.; Xu, H.; Shou, C. Prognostic Significance of Phosphatase of Regenerating Liver-3 Expression in Ovarian Cancer. *Pathol. Oncol. Res.* **2009**, *15*, 555−560.

(7) Vandsemb, E. N.; Bertilsson, H.; Abdollahi, P.; Størkersen, Ø.; Våtsveen, T. K.; Rye, M. B.; Rø, T. B.; Børset, M.; Slørdahl, T. S. Phosphatase of regenerating liver 3 (PRL-3) is overexpressed in human prostate cancer tissue and promotes growth and migration. *J. Transl. Med.* **2016**, *14*, 71.

(8) Luján, P.; Varsano, G.; Rubio, T.; Hennrich, M. L.; Sachsenheimer, T.; Gálvez-Santisteban, M.; Martín-Belmonte, F.; Gavin, A. C.; Brügger, B.; Köhn, M. PRL-3 disrupts epithelial architecture by altering the post-mitotic midbody position. *J. Cell Sci.* **2016**, *129*, 4130−4142.

(9) Abdollahi, P.; Vandsemb, E. N.; Børset, M. Phosphatases of regenerating liver are key regulators of metabolism in cancer cells - role of Serine/Glycine metabolism. *Curr. Opin. Clin. Nutr. Metab. Care* **2022**, *25*, 50−55.

(10) Abdollahi, P.; Vandsemb, E. N.; Elsaadi, S.; Røst, L. M.; Yang, R.; Hjort, M. A.; Andreassen, T.; Misund, K.; Slørdahl, T. S.; Rø, T. B.; et al. Phosphatase of regenerating liver-3 regulates cancer cell metabolism in multiple myeloma. *Fed. Am. Soc. Exp. Biol. J.* **2021**, *35*, No. e21344.

(11) Ming, J.; Jiang, Y.; Jiang, G.; Zheng, H. Phosphatase of Regenerating Liver-3 Induces Angiogenesis by Increasing Extracellular Signal-Regulated Kinase Phosphorylation in Endometrial Adenocarcinoma. *Pathobiology* **2013**, *81*, 1−7.

(12) Laura, D.; Luis, C.; Maria, K.; Inna, K.; Simon, S. The Phosphatase PRL-3 Is Involved in Key Steps of Cancer Metastasis. *J. Mol. Biol.* **2019**, *431*, 3056−3067.

(13) Funato, Y.; Yamazaki, D.; Mizukami, S.; Du, L.; Kikuchi, K.; Miki, H. Membrane protein CNNM4−dependent Mg2+ efflux suppresses tumor progression. *J. Clin. Invest.* **2014**, *124*, 5398−5410.

(14) Hardy, S.; Uetani, N.; Wong, N.; Kostantin, E.; Labbé, D. P.; Bégin, L. R.; Mes-Masson, A.; Miranda-Saavedra, D.; Tremblay, M. L. The protein tyrosine phosphatase PRL-2 interacts with the magnesium transporter CNNM3 to promote oncogenesis. *Oncogene* **2015**, *34*, 986−995.

(15) Gulerez, I.; Funato, Y.; Wu, H.; Yang, M.; Kozlov, G.; Miki, H.; Gehring, K. Phosphocysteine in the PRL-CNNM pathway mediates magnesium homeostasis. *Eur. Mol. Biol. Organ. Rep.* **2016**, *17*, 1890−1900.

(16) Zhang, H.; Kozlov, G.; Li, X.; Wu, H.; Gulerez, I.; Gehring, K. PRL3 phosphatase active site is required for binding the putative magnesium transporter CNNM3. *Sci. Rep.* **2017**, *7*, 48.

(17) Chen, Y. S.; Kozlov, G.; Fakih, R.; Funato, Y.; Miki, H.; Gehring, K. The cyclic nucleotide−binding homology domain of the integral membrane protein CNNM mediates dimerization and is required for Mg2+ efflux activity. *J. Biol. Chem.* **2018**, *293*, 19998−20007.

(18) Funato, Y.; Miki, H. Molecular function and biological importance of CNNM family Mg2+ transporters. *J. Biochem.* **2019**, *165*, 219−225.

(19) Giménez-Mascarell, P.; González-Recio, I.; Fernández-Rodríguez, C.; Oyenarte, I.; Müller, D.; Martínez-Chantar, M.; Martínez-Cruz, L. Current Structural Knowledge on the CNNM Family of Magnesium Transport Mediators. *Int. J. Mol. Sci.* **2019**, *20*, 1135.

(20) Chen, Y. S.; Kozlov, G.; Fakih, R.; Yang, M.; Zhang, Z.; Kovrigin, E. L.; Gehring, K. Mg2+-ATP Sensing in CNNM, a Putative Magnesium Transporter. *Structure* **2020**, *28*, 324.e4−335.e4.

(21) Bai, Z.; Feng, J.; Franken, G. A. C.; Al'Saadi, N.; Cai, N.; Yu, A. S.; Lou, L.; Komiya, Y.; Hoenderop, J. G. J.; De Baaij, J. H. F.; et al. CNNM proteins selectively bind to the TRPM7 channel to stimulate divalent cation entry into cells. *PLoS Biol.* **2021**, *19*, No. e3001496.

(22) Giménez-Mascarell, P.; Oyenarte, I.; Hardy, S.; Breiderhoff, T.; Stuiver, M.; Kostantin, E.; Diercks, T.; Pey, A. L.; Ereño-Orbea, J.; Martínez-Chantar, M. L.; et al. Structural Basis of the Oncogenic Interaction of Phosphatase PRL-1 with the Magnesium Transporter CNNM2. *J. Biol. Chem.* **2017**, *292*, 786−801.

(23) Kozlov, G.; Funato, Y.; Chen, Y. S.; Zhang, Z.; Illes, K.; Miki, H.; Gehring, K. PRL3 pseudophosphatase activity is necessary and sufficient to promote metastatic growth. *J. Biol. Chem.* **2020**, *295*, 11682−11692.

(24) Trapani, V.; Wolf, F. Dysregulation of Mg2+ homeostasis contributes to acquisition of cancer hallmarks. *Cell Calcium* **2019**, *83*, No. 102078.

(25) Kostantin, E.; Hardy, S.; Valinsky, W. C.; Kompatscher, A.; De Baaij, J. H. F.; Zolotarov, Y.; Landry, M.; Uetani, N.; Martínez-Cruz, L. A.; Hoenderop, J. G. J.; et al. Inhibition of PRL-2·CNNM3 Protein

Complex Formation Decreases Breast Cancer Proliferation and Tumor Growth. *J. Biol. Chem.* **2016**, *291*, 10716−10725.
(26) Kozlov, G.; Cheng, J.; Ziomek, E.; Banville, D.; Gehring, K.; Ekiel, I. Structural Insights into Molecular Function of the Metastasis-associated Phosphatase PRL-3. *J. Biol. Chem.* **2004**, *279*, 11882−11889.
(27) Hardy, S.; Kostantin, E.; Wang, S. J.; Hristova, T.; Galicia-Vázquez, G.; Baranov, P. V.; Pelletier, J.; Tremblay, M. L. Magnesium-sensitive upstream ORF controls PRL phosphatase expression to mediate energy metabolism. *Proc. Natl. Acad. Sci. U. S. A.* **2019**, *116*, 2925−2934.
(28) Gungabeesoon, J.; Tremblay, M. L.; Uetani, N. Localizing PRL-2 expression and determining the effects of dietary Mg(2+) on expression levels. *Histochem. Cell Biol.* **2016**, *146*, 99−111.
(29) Kochańczyk, T.; Nowakowski, M.; Wojewska, D.; Kocyła, A.; Ejchart, A.; Koźmiński, W.; Krężel, A. Metal-coupled folding as the driving force for the extreme stability of Rad50 zinc hook dimer assembly. *Sci. Rep.* **2016**, *6*, 36346.
(30) Dean, R. L. Kinetic studies with alkaline phosphatase in the presence and absence of inhibitors and divalent cations. *Biochem. Mol. Biol. Educ.* **2002**, *30*, 401−407.
(31) Bellomo, E.; Singh, K. B.; Massarotti, A.; Hogstrand, C.; Maret, W. The Metal Face of Protein Tyrosine Phosphatase 1B. *Coord. Chem. Rev.* **2016**, *327*, 70.
(32) Monteilh-Zoller, M. K.; Hermosura, M. C.; Nadler, M. J. S.; Scharenberg, A. M.; Penner, R.; Fleig, A. TRPM7 Provides an Ion Channel Mechanism for Cellular Entry of Trace Metal Ions. *J. Gen. Physiol.* **2003**, *121*, 49−60.
(33) Mittermeier, L.; Demirkhanyan, L.; Stadlbauer, B.; Breit, A.; Recordati, C.; Hilgendorff, A.; Matsushita, M.; Braun, A.; Simmons, D. G.; Zakharian, E.; et al. TRPM7 is the central gatekeeper of intestinal mineral absorption essential for postnatal survival. *Proc. Natl. Acad. Sci. U. S. A.* **2019**, *116*, 4706−4715.
(34) Mellott, A. N. *Divalent Metal Cation Entry and Cytotoxicity in Jurkat T Cells: Role of TRPM7 Channels*; Wright State University, 2020. http://rave.ohiolink.edu/etdc/view?acc_num=wright1597319673881729.
(35) McParland, V.; Varsano, G.; Li, X.; Thornton, J.; Baby, J.; Aravind, A.; Meyer, C.; Pavic, K.; Rios, P.; Köhn, M. The Metastasis-Promoting Phosphatase PRL-3 Shows Activity toward Phosphoinositides. *Biochemistry* **2011**, *50*, 7579−7590.
(36) Hardy, S.; Zolotarov, Y.; Coleman, J.; Roitman, S.; Khursheed, H.; Aubry, I.; Uetani, N.; Tremblay, M. L. PRL-1/2 phosphatases control TRPM7 magnesium-dependent function to regulate cellular bioenergetics. *Proc. Natl. Acad. Sci. U. S. A.* **2023**, *120*, No. e2221083120.
(37) Kim, K. A.; Song, J. S.; Jee, J.; Sheen, M. R.; Lee, C.; Lee, T. G.; Ro, S.; Cho, J. M.; Lee, W.; Yamazaki, T.; et al. Structure of human PRL-3, the phosphatase associated with cancer metastasis. *Fed. Eur. Biochem. Soc., Lett.* **2004**, *565*, 181−187.
(38) Stefan, W.; Karl-Heinz, B.; Wolfgang, S.; Günter, M.; Stefan, P.; Norbert, T. 6,8-Difluoro-4-methylumbiliferyl phosphate: a fluorogenic substrate for protein tyrosine phosphatases. *Anal. Biochem.* **2005**, *338*, 32−38.
(39) Diamond, R. H.; Cressman, D. E.; Laz, T. M.; Abrams, C. S.; Taub, R. PRL-1, a unique nuclear protein tyrosine phosphatase, affects cell growth. *Mol. Cell. Biol.* **1994**, *14*, 3752−3762.
(40) Elise Burmeister, G.; Ming, X.; Tania, C.; Roger, C.; Paul, R. S. A Comparison between the Sulfhydryl Reductants Tris(2-carboxyethyl)phosphine and Dithiothreitol for Use in Protein Biochemistry. *Anal. Biochem.* **1999**, *273*, 73−80.
(41) Pace, N.; Weerapana, E. Zinc-Binding Cysteines: Diverse Functions and Structural Motifs. *Biomolecules* **2014**, *4*, 419−434.
(42) Krężel, A.; Maret, W. Zinc-buffering capacity of a eukaryotic cell at physiological pZn. *J. Biol. Inorg. Chem.* **2006**, *11*, 1049−1062.
(43) Vinkenborg, J. L.; Nicolson, T. J.; Bellomo, E. A.; Koay, M. S.; Rutter, G. A.; Merkx, M. Genetically encoded FRET sensors to monitor intracellular Zn2+ homeostasis. *Nat. Methods* **2009**, *6*, 737−740.
(44) Xiong, Y.; Luo, D. J.; Wang, X. L.; Qiu, M.; Yang, Y.; Yan, X.; Wang, J. Z.; Ye, Q. F.; Liu, R. Zinc binds to and directly inhibits protein phosphatase 2A *in vitro*. *Neurosci. Bull.* **2015**, *31*, 331−337.
(45) Wilson, M.; Hogstrand, C.; Maret, W. Picomolar concentrations of free zinc(II) ions regulate receptor protein-tyrosine phosphatase β activity. *J. Biol. Chem.* **2012**, *287*, 9322−9326.
(46) Cai, F.; Huang, Y.; Wang, M.; Sun, M.; Zhao, Y.; Hattori, M. A FRET-based screening method to detect potential inhibitors of the binding of CNNM3 to PRL2. *Sci. Rep.* **2020**, *10*, 12879.
(47) Niyogi, S. K.; Feldman, R. P.; Hoffman, D. J. Selective effects of metal ions on RNA synthesis rates. *Toxicology* **1981**, *22*, 9−21.
(48) Smethurst, D. G. J.; Shcherbik, N. Interchangeable utilization of metals: New perspectives on the impacts of metal ions employed in ancient and extant biomolecules. *J. Biol. Chem.* **2021**, *297*, No. 101374.
(49) Freudenrich, C. C.; Murphy, E.; Levy, L. A.; London, R. E.; Lieberman, M. Intracellular pH modulates cytosolic free magnesium in cultured chicken heart cells. *Am. J. Physiol.* **1992**, *262*, C1024−C1030.
(50) Waldron, K. J.; Rutherford, J. C.; Ford, D.; Robinson, N. J. Metalloproteins and metal sensing. *Nature* **2009**, *460*, 823−830.
(51) Korotkova, N.; Freire, D.; Phan, T. H.; Ummels, R.; Creekmore, C. C.; Evans, T. J.; Wilmanns, M.; Bitter, W.; Parret, A. H.; Houben, E. N.; et al. Structure of the Mycobacterium tuberculosis type VII secretion system chaperone EspG5 in complex with PE25-PPE41 dimer. *Mol. Microbiol.* **2014**, *94*, 367−382.
(52) Rivas, D. R.; Dela Cerna, M. V. C.; Smith, C. N.; Sampathi, S.; Patty, B. G.; Lee, D.; Blackburn, J. S. A screen of FDA-approved drugs identifies inhibitors of protein tyrosine phosphatase 4A3 (PTP4A3 or PRL-3). *Sci. Rep.* **2021**, *11*, 10302.
(53) Julie, L. B.; Rachel, G. Chapter Thirteen - Coomassie Blue Staining. In *Laboratory Methods in Enzymology: Protein Part C*, Jon, L. Ed.; Academic Press, 2014; Vol. *541*, pp 161−167.
(54) Lu, C.-H.; Chen, C.-C.; Yu, C.-S.; Liu, Y.-Y.; Liu, J.-J.; Wei, S.-T.; Lin, Y.-F. MIB2: metal ion-binding site prediction and modeling server. *Bioinformatics* **2022**, *38*, 4428−4429. (acccessed January 28, 2023).
(55) Micsonai, A.; Moussong, É.; Wien, F.; Boros, E.; Vadászi, H.; Murvai, N.; Lee, Y.-H.; Molnár, T.; Réfrégiers, M.; Goto, Y.; et al. BeStSel: webserver for secondary structure and fold prediction for protein CD spectroscopy. *Nucleic Acids Res.* **2022**, *50*, W90−W98. (acccessed January 29, 2023).
(56) Bender, M. L.; Kezdy, F. J.; Wedler, F. C. alpha-Chymotrypsin: Enzyme concentration and kinetics. *J. Chem. Educ.* **1967**, *44*, 84.
(57) Schindelin, J.; Arganda-Carreras, I.; Frise, E.; Kaynig, V.; Longair, M.; Pietzsch, T.; Preibisch, S.; Rueden, C.; Saalfeld, S.; Schmid, B.; et al. Fiji: an open-source platform for biological-image analysis. *Nat. Methods* **2012**, *9*, 676−682.

https://doi.org/10.1021/acsomega.3c04095
ACS Omega 2023, 8, 30578−30589